# Real-time Cycle-slip Detection and Correction for Land Vehicle Navigation using Inertial Aiding

Malek O. Karaim, *Queen's University*
Tashfeen B. Karamat, *Queen's University*
Aboelmagd Noureldin, *Royal Military College of Canada and Queen's University*
Mohamed Tamazin, *Queen's University*
Mohamed M. Atia, *Royal Military College of Canada*

## BIOGRAPHY

Malek Karaim is a Ph.D. student at the Department of Electrical and Computer Engineering, Queen's university, Canada. Malek is working in the area of GPS/INS integration within the Navigation and Instrumentation Research (NavINST) Group at Queens' University/Royal Military College of Canada. His current research involves cycle slip detection and correction using inertial aiding.

Tashfeen Karamat is a Ph.D. candidate at the Department of Electrical and Computer Engineering, Queen's University, Canada. His research involves optimal data fusion techniques based on Kalman filtering for GPS/INS integration. Currently, he is working on optimizing integer ambiguity resolution using inertial aiding.

Aboelmagd Noureldin is a cross-appointment associate professor at the departments of electrical and computer engineering in Queen's University and the Royal Military College (RMC) of Canada. His research is related to artificial intelligence, digital signal processing, and estimation with emphasis on their applications to INS/GPS. He is the director of the Navigation and Instrumentation Research Group at RMC.

Mohamed Tamazin is a PhD candidate in the Navigation and Instrumentation (NavINST) group of the Department of Electrical and Computer Engineering in Queen's University, Ontario, Canada. His research interests in the fields of GNSS signal processing, software receiver design and integrated navigation systems.

Mohamed M. Atia is currently Research Associate and Deputy Director of Navigation & Instrumentation Lab in Royal Military College of Canada. In the past few years, Dr.Atia gained extensive industry proven experience in designing, architecting, and leading the research and development of navigation systems for different operating systems including embedded systems and portable devices.

## ABSTRACT

Carrier phase measurements require resolution of integer ambiguities before precise positioning can be achieved. The GPS receiver can keep track of the integer number of cycles as long as the receiver maintains lock to the satellite signal. However, in reality, the GPS signal could be interrupted momentary by some disturbing factors leading to a discontinuity of an integer number of cycles in the measured carrier phase. This interruption in the counting of cycles in the carrier phase measurements is known as a cycle slip. After a cycle slip, ambiguities need to be resolved again or cycle slips need to be corrected to resume the precise positioning/navigation process. These cycle slips can, to some extent, be detected and fixed to avoid delay and computation complexity attributed to the process of integer ambiguity resolution. Capitalizing on the complementary characteristics of INS and GPS, INS is used to provide external information to detect and correct cycle slips. Lately, MEMS grade inertial sensors are being used for low cost navigation applications. Moreover, recent research is geared towards the use of fewer numbers of sensors avoiding their complex errors and reducing the cost. This paper introduces integration of GPS and reduced inertial sensor system (RISS) to address the problem of cycle slips. The performance of proposed method is examined on several real-life land vehicle trajectories which included various challenging driving scenarios including high and slow speeds, sudden accelerations and decelerations, sharp turns and steep slopes etc. Results demonstrate the effectiveness of the proposed algorithm in these severe conditions which cause intensive and variable-sized cycle slips. This research has a direct influence on navigation in challenging environments where frequent cycle slips occur and resolving integer ambiguities is not affordable because of time and computational constraints. An additional consequence of this research is the significant reduction in the cost of an integrated system due to the use of fewer MEMS inertial sensors.

## INTRODUCTION

In Global Positioning System (GPS), carrier phase measurements can be used to achieve very precise positioning solutions. Carrier phase measurements are much more precise than pseudorange measurements but they are ambiguous by an integer number of cycles. When these ambiguities are resolved, a sub-centimetre level positioning can be achieved. However, in real-time kinematic applications, the GPS signal could temporarily be lost because of various disturbing factors such as trees, buildings, bridges and vehicle dynamics [1] [2]. This signal loss causes a discontinuity of an integer number of cycles in the measured carrier phase, known as cycle slip. Consequently, the integer counter is reinitialized, meaning that the integer ambiguities become unknown again. In this event, ambiguities need to be resolved once more to resume the precise positioning and navigation process. This is a computation-intensive and time-consuming task [3]. Typically, it takes at least few minutes to resolve for ambiguities. The ambiguity resolution is even more challenging in real-time navigation due to the receiver dynamics and time sensitive nature of the required kinematic solution. Therefore, it would save effort and time if we could detect and estimate the size of these cycle slips and correct the measurements accordingly instead of resorting ambiguity resolution.

## CYCLE SLIPS AND THEIR MANAGMENT

GPS signal is very weak and could be interrupted momentary by some disturbing factors leading to a discontinuity of an integer number of cycles in the measured carrier phase as a result of a temporary loss-of-lock in the phase tracking loops [4] [5]. This discontinuity in the integer number of cycles is known as a cycle slip. A cycle slip causes a jump in the carrier phase measurements whereas pseudoranges remain unaffected as graphically depicted in Figure 1. When a cycle slip happens, the Doppler counter would restart, causing a jump in the instantaneous accumulated phase by an integer number of cycles. Thus, the integer counter is reinitialized, meaning that ambiguities are unknown again producing a sudden change in the carrier phase observations.

Once a cycle slip is detected, there are two ways to handle it [6]. One way is to repair the slips while the other is to reinitialize the unknown ambiguity parameter in phase measurements. The former technique requires exact estimation of the size of the slip but could be done instantaneously. The latter solution is more secure [1] but it is time-consuming and computation-intensive [3]. In this work we follow the first approach providing a real time cycle slip detection and correction algorithm based on GPS/RISS integration scheme.

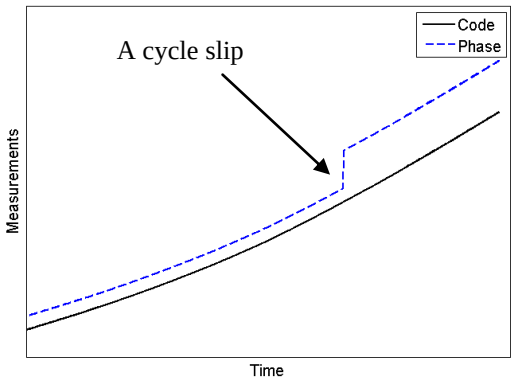


Figure 1: A cycle slip affecting phase measurements but not the pseudoranges

## REDUCED INERTIAL SENSOR SYSTEM (RISS)

Recently, the Micro Electro Mechanical Systems (MEMS) grade inertial sensors are being used for low cost navigation applications. However, these inexpensive sensors have complex error characteristics; therefore, latest research is directed towards the utilization of fewer numbers of inertial sensors inside the inertial measurement unit (IMU) to obtain the navigation solution [7]. Advantage of this trend is twofold. The first is to avoid the effect of the inertial sensor errors. The second is to reduce the cost of the IMU in general [8]. One such approach is used in this work known as the RISS (Reduced Inertial Sensor System). The RISS configuration uses one gyroscope, two accelerometers, and vehicle wheel rotation sensor. The gyroscope is used to observe the changes in vehicle's orientation in the horizontal plane. The two accelerometers are used to obtain the pitch and roll angles. The wheel rotation sensor readings provide the vehicle's speed in the forward direction. A general view of the RISS configuration is given in Figure 2.

## GPS/INS INTEGRATION

Inertial Navigation Systems (INS) can provide a smoother and continuous navigation solution at higher data rates since it is autonomous and immune to interferences that deteriorates the GPS positioning quality. However, INS errors grow with time due to inherent integration in the mechanization process. Thus, both GPS and INS systems exhibit mutually complementary characteristics, and their integration provides a more accurate and robust navigation solution than either stand-alone system [9] [10]. GPS/INS integration is often implemented using a filtering technique. Kalman filter is typically selected for its estimation optimality and time recursion properties.

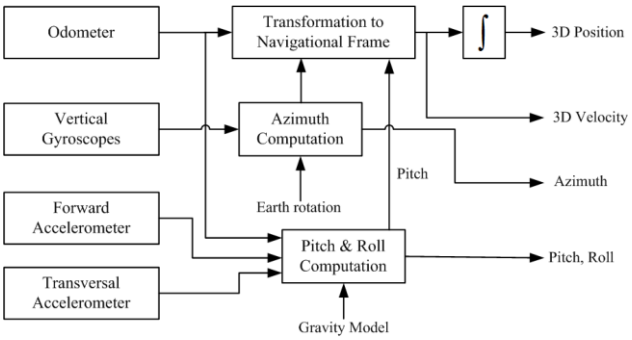


Figure 2: A general view of the RISS configuration

Major approaches of integration are loosely coupled GPS/INS integration and tightly coupled GPS/INS integration. The former strategy is simpler and easier to implement since the inertial and GPS navigation solutions are generated independently before being weighted together by the Kalman filter. There are two main drawbacks with this approach: 1) signals from at least four satellites are needed for navigation solution which cannot always be guaranteed; and 2) the outputs of the GPS Kalman filter are time correlated which has a negative impact upon the system performance. The latter strategy performs the INS/GPS integration in a single centralized Kalman filter. This architecture eliminates the problem of correlated measurements which arises due to cascaded Kalman filtering in the loosely coupled approach. Moreover, the restriction of visibility of at least four satellites is removed. It may be noted that we use RISS which is integrated with GPS as shown in Figure 3.

A tightly-coupled GPS/RISS is used in this work as shown in Figure 3. In this three-dimension (3D) version of RISS, the system has a total of eleven states; nine states from RISS side and two more states are added from the GPS side. These states are latitude, longitude and altitude errors $(\delta\varphi, \delta\lambda, \delta h)$; the East, North and Up velocity errors $(\delta v_e, \delta v_n, \delta v_u)$; the azimuth error $(\delta A)$; the error associated with odometer-driven acceleration $(\delta a_{od})$; and the gyroscope error $(\delta\omega_z)$. The additional two states are bias $\delta b_r$ $(\delta b_r)$ and drift $(\delta d_r)$ of the GPS receiver. Details of GPS/RISS equations and derivations can be found in [11] [12] [13].

The nine-state error vector $x_k$ at time $t_k$ is expressed as:

$$x_k = (\delta\phi, \delta\lambda, \delta h, \delta v_e, \delta v_n, \delta v_u, \delta A, \delta a_{od}, \delta\omega_z) \quad (1)$$

## CYCLE SLIP DETECTION AND CORRECTION

Cycle slip detection and correction usually happens in two steps, detection and fixing [1] [3]. In the first step, using some testing quantity, the location (time) of the slip is found. During the second step, the size of the slip is determined which is needed along with its location to fix the cycle slip. Various techniques have been introduced address the problem of cycle slip detection and correction. measurement-combinations are used including phase-code (L1 or L2), phase-phase (Dual frequency L1 and L2), Doppler (L1 or L2), and time-differential phases (L1 or L2) [1] [6]. In GPS/INS integration systems, INS is used to predict the required variable to test for cycle slip, which is usually the true receiver-to-satellite range in DD mode [14] [15]. In this paper, a tightly coupled GPS/RISS integrated system is introduced for cycle slip detection and correction for land vehicle navigation using relative-positioning technique.

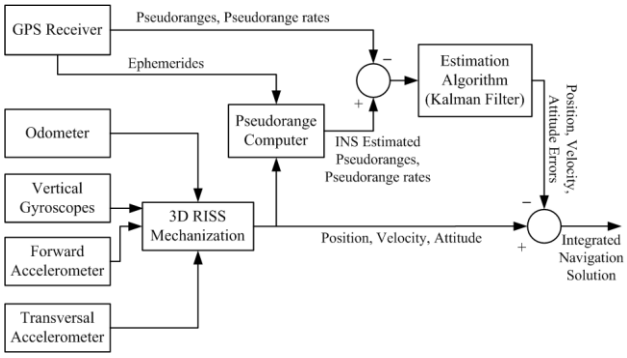


Figure 3: Tightly coupled integration of GPS/RISS

## PRINCIPLE OF THE ALGORITHM

The proposed algorithm compares double differenced (DD) phase measurements with estimated measurements derived from the output of the GPS/RISS system. In case of a cycle slip, the measurements are corrected with the calculated difference. A general overview of the system is given in Figure 4.

$$\Delta N(t) = \Delta\nabla\phi(t) - \Delta\nabla\hat{\phi}(t) \quad (2)$$

Where

$\Delta N(t)$ is the number of slipped cycles

$\Delta\nabla\phi(t)$ is DD phase measurements

$\Delta\nabla\hat{\phi}(t)$ is DD estimated phase

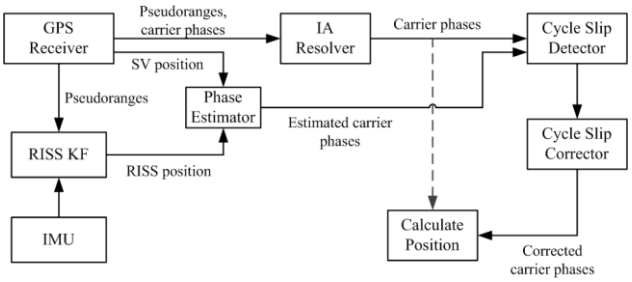


Figure 4: The general flow diagram of the proposed algorithm

$\Delta N(t)$ is compared to a threshold $\mu$. If the threshold is exceeded, it indicates that there is a cycle slip in the DD phase measurements. Theoretically, $\Delta N(t)$ would be an integer but because of the errors in the measured phase as well as errors in the estimations coming from the INS system, $\Delta N(t)$ will most likely be a float number.

The estimated phase term in equation (2) is obtained as follows:

$$\Delta\nabla\hat{\phi}(t) = \frac{1}{\lambda}\left\{\left[\hat{r}_R^i(t) - r_B^i(t)\right] - \left[\hat{r}_R^j(t) - r_B^j(t)\right]\right\} \qquad (3)$$

Where

$\lambda$ is the wavelength of the carrier signal

$\hat{r}_R^i(t), r_R^j(t)$ are estimated ranges from rover to satellites $i$ and $j$ respectively, (meters)

$\hat{r}_B^i(t), r_B^j(t)$ are known ranges from base to $i$ and $j$ satellites respectively, (meters)

What we need to get from the integrated GPS/RISS system is estimated ranges vector from receiver to each available satellite $(\hat{r}_R^1, \hat{r}_R^2, \cdots, \hat{r}_R^m)$. Knowing our best position estimation, we can calculate ranges from the receiver to all available satellites through:

$$\hat{\mathbf{r}}_R^m = \left\| \mathbf{x}^{KF} - \mathbf{x}^m \right\|, \; m = 1, ..., M \qquad (4)$$

Where

$\hat{\mathbf{r}}_R^m$ is the calculated range from receiver to $m^{th}$ satellite

$\mathbf{x}^{KF}$ is the receiver position obtained from GPS/RISS Kalman filter solution

$\mathbf{x}^m$ is the position of $m^{th}$ satellite

$M$ is the number of available satellites

Then, estimated DD phase term in equation (3) can be calculated and the following test quantity in equation (2) can be applied.

$$\Delta N^i(t) = \Delta\nabla\phi^i(t) - \Delta\nabla\hat{\phi}^i(t), \quad i = 1, ..., M-1 \qquad (5)$$

Table 1: Characteristics of Crossbow and Honeywell IMUs

| | *Crossbow* | *HG1700* |
|---|---|---|
| Size (cm) | 7.62x9.53x8.13 | 16 x 16 x 10 |
| Weight | 0.59 kg | 0.725 kg |
| Max Data Rate | 200 Hz | 100 Hz |
| *Gyroscope* | | |
| Range | ± 100 °/s | ± 1000 °/s |
| Bias | < ± 2.0 °/s | 1 °/hr |
| Scale Factor | < 1 % | 150 ppm |
| Random Walk | <2.25 °/$\sqrt{hr}$ | <0.125 °/$\sqrt{hr}$ |
| *Accelerometer* | | |
| Range | ± 2 g | ± 50 g |
| Bias | ± 30 mg | 1.0 mg |
| Scale Factor | < 1 % | 300 ppm |
| Random Walk | <0.15 m/s/$\sqrt{hr}$ | <0.198 m/s/$\sqrt{hr}$ |

If a cycle slip occurred in the $i^{th}$ DD phase-set, the corresponding set is instantly corrected for that slip by:

$$\Delta\nabla\phi^s(t) = \Delta\nabla\phi^s(t) - \Delta N^i(t) \qquad (6)$$

Where $s$ is the DD phase-set number in which the cycle slip has occurred.

## EXPERIMENTAL WORK

The performance of the proposed algorithm was examined on the data collected from several real land vehicle trajectories. The Honeywell HG1700 AG11 high end tactical grade IMU was integrated with a NovAtel OEM4 GPS receiver to provide the reference solution. The HG1700 AG11 IMU unit uses three ring-laser gyroscopes and three accelerometers mounted orthogonally to measure angular rate and linear acceleration. The Novatel OEM4 GPS receiver and the Honeywell HG1700 AG11 systems were integrated through a G2 Pro-Pack SPAN unit developed by Novatel Inc. For the GPS/RISS solution, a NovAtel OEM4 GPS receiver and a Crossbow IMU300CC MEMS grade IMU were used. The IMU300CC IMU is a six degree of freedom inertial system but data from only vertical gyroscope, forward accelerometer, and transversal accelerometer was used. Table 1 gives the main characteristics of both IMU units. The odometer data was collected using a CarChip data logger through on-board diagnostics version II interface. Another NovAtel OEM4 GPS receiver was used for the base station measurements. The GPS data was logged at 1Hz. Figure 5 shows some data collection equipment setup used during road test trajectories.

Several road trajectories were conducted using the above described configuration. One of the trajectories, which covers several real-life scenarios encountered in a typical road journey is selected to show the performance of the proposed algorithm. The trajectory was carried out in the city of Kingston, ON, Canada. The starting and end point was near the well surveyed point at Fort Henry National Historic Site where the base station receiver was located. The length of the trajectory was about 30 minutes and the total distance traveled was about 33 Km and maximum base line length was about 15 Km. The trajectory incorporated a portion of highway 401 with a maximum speed limit of 100km/h and suburban areas with max speed limit of 80km/h. It also contained different scenarios including sharp turns, high speeds and slopes.

Some statistics are given in this section to describe the selected road test trajectory. Figure 6 shows measured phase at the rover for the different satellites. Some satellites show very poor presence whereas few others are consistently available. Satellites elevations can be seen in Figure 7.

## RESULTS

We start with showing some results of phase estimation errors. Processing is done on what is considered to be a cycle-slip-free portion of the data set for some persistent satellites (usually with moderate to higher elevations). Then we show, results for the cycle slip detection process by introducing cycle slips in different scenarios. In the ensuing discussion (including tables and figures) we mention and show results indicating satellite numbers without any mention of reference satellites, which should be implicit as we are dealing with DD data.

Figure 8 and Figure 9 show DD-Phase estimation errors whereas Figure 10 and Figure 11 show DD measured phases versus DD estimated phases for sample satellites, number 22 and 27. As it can be seen in Table 2, RMS error varies from 0.93 to 3.58 cycles with standard deviation from 0.85 to 2.47 cycles. Estimated phases are approximately identical to the measured ones. Nevertheless, most of the DD phase estimations have bias and general drift trends which need some elaboration. In fact, the bias error can be the result of more than one cause. The low cost inertial sensors always have bias in their characteristics which plays a major role in this. The drift is further affecting relatively lower elevation satellites which can also be attributed to more than one reason. Indeed, one reason of choosing this specific trajectory which was conducted in 2011 was to test the algorithm with severe ionospheric conditions as the year 2011 was close to a solar maximum: a period of peak solar activity in the 11 year solar cycle of the Sun.

Figure 5: Data collection equipment mounted inside the road test vehicle

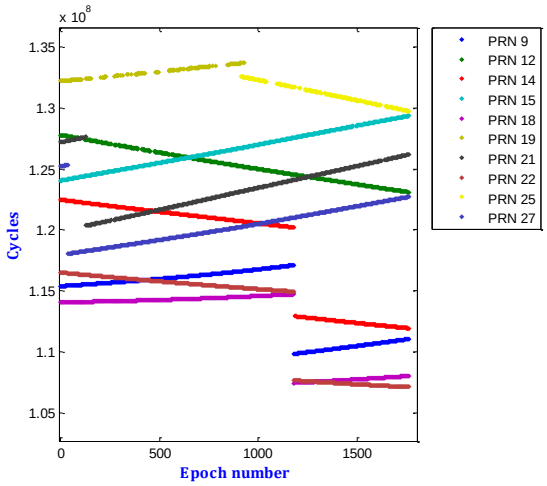


Figure 6: Measured phase at the rover

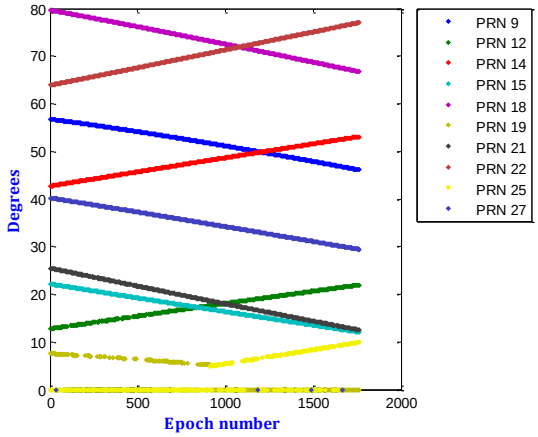


Figure 7: Satellites elevations

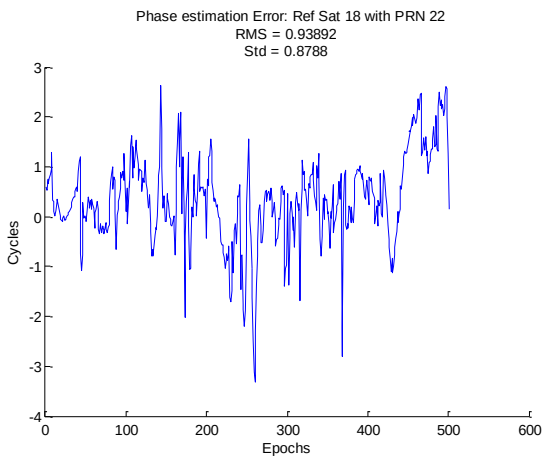


Figure 8: DD-Phase estimation error Ref Sat with PRN 22

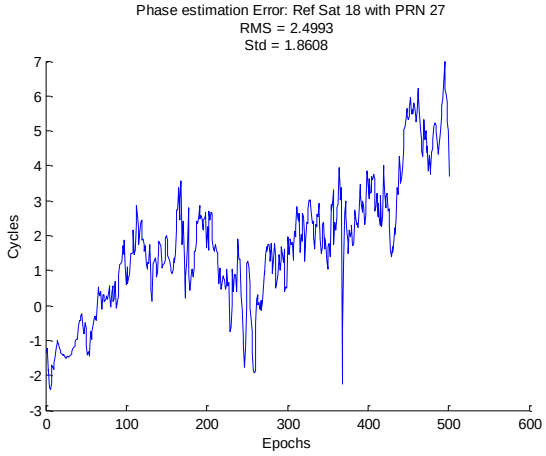


Figure 9: DD-Phase estimation error Ref Sat with PRN 27

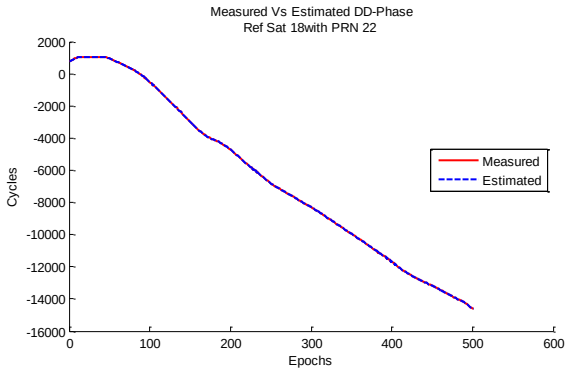


Figure 10: Measured versus estimated DD-Phase Ref Sat with PRN 22

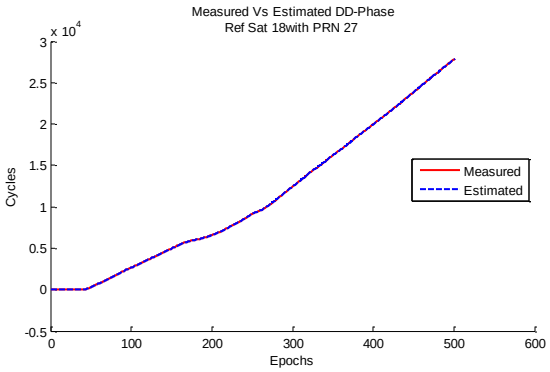


Figure 11: Measured versus estimated DD-Phase Ref Sat with PRN 27

Moreover, trajectory time was in the afternoon which has the maximum ionospheric effects during the day. Thus, most part of the drift trend must be coming from ionospheric effects as the rover is moving away from the base receiver during this portion of the trajectory. Besides, satellites geometry could contribute to this error component. Most of the sudden jumps are coinciding with or following sharp vehicle turns and rapid tilts. Table 2 shows the averaged RMS DD phase estimation error for the sample satellite-pairs. We introduced cycle slips in different intensities and sizes to simulate real life scenarios. Fortunately, cycle slips are usually big as mentioned earlier and corroborated by our observations from real trajectory data. Therefore, it is more important to detect and correct for bigger slips in general.

Table 2: Phase estimation error for DD phases

| Satellite pair | RMS | std (cycles) |
|---|---|---|
| Ref-PRN 9 | 1.15 | 0.85 |
| Ref-PRN 14 | 1.45 | 1.38 |
| Ref-PRN 18 | 3.58 | 2.47 |
| Ref-PRN 22 | 0.93 | 0.87 |
| Ref-PRN 27 | 2.49 | 1.86 |

## INTRODUCING AND DETECTING CYCLE SLIPS

To test the robustness of the algorithm, we started with an adequate cycle slip size. Cycle slips of size 10-1000 cycles were introduced with different intensities. These intensities are categorized as *few* (1 slip/100 Epochs), *moderate* (10 slip/100 Epochs) and *severe* (100 slip/100 Epochs) were selected. This was applied for all DD phases measurement sets simultaneously. Threshold was set to 1.9267 (average of RMS error for all satellite-pairs) cycles. Four metrics were used to describe the results. Mean square error (MSE); *accuracy*, the detected cycle slip size with respect to the introduced size; True Detection (TD) ratio; and Mis-detection (MD) ratio. For limited space and similarity between results for different

satellites, we only show results for reference satellite with only PRN 15 and PRN 22. Figure 12 to Figure 17 show introduced versus calculated cycle slips along with the corresponding detection error for sample satellites in the different scenarios. Table 3 to
Table 5 summarize these results.

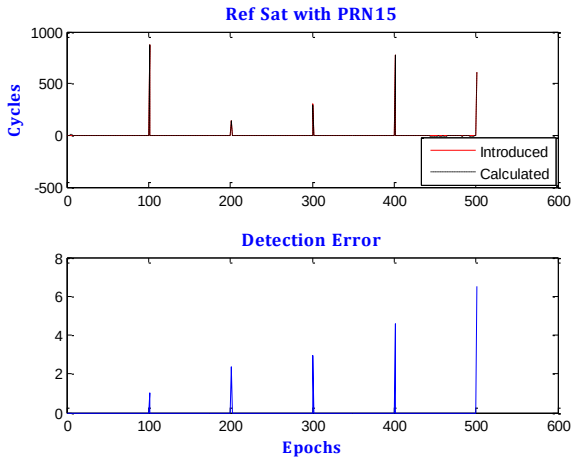


Figure 12: Few cycle slips Ref Sat with PRN 15

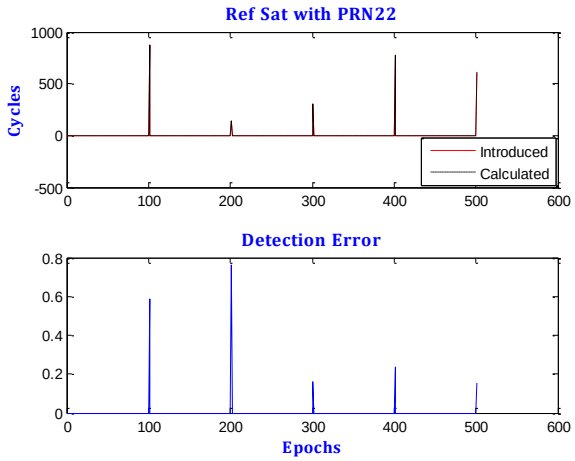


Figure 13: Few cycle slips Ref Sat with PRN 22

All introduced cycle slips were successfully detected in all few, moderate, and severe cases with very high accuracy. Slight change in the accuracy (increasing with higher intensity) among the different scenarios show that detection accuracy is not affected by cycle slips intensity. Higher *mis-detection* ratio for less cycle slips intensity is coming from bigger error margins than the threshold for several satellite-pairs. However, this is not affecting the overall accuracy strongly as all mis-detected slips are of comparably very smaller sizes. MD ratio is zero in the intensive cycle slip case as all epochs contain slips is an indicator of performance compromise with slips intensity.

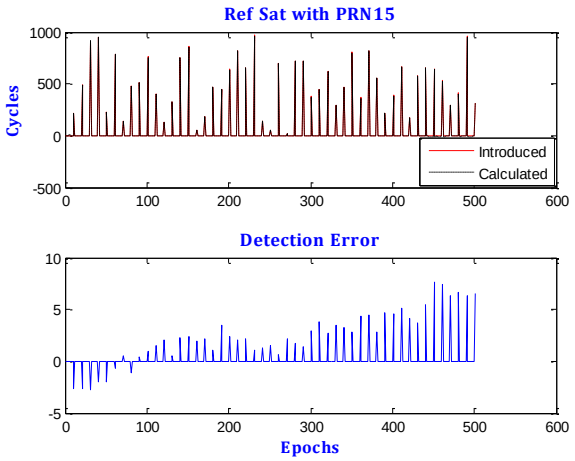


Figure 14: Moderate cycle slips Ref Sat with PRN 15

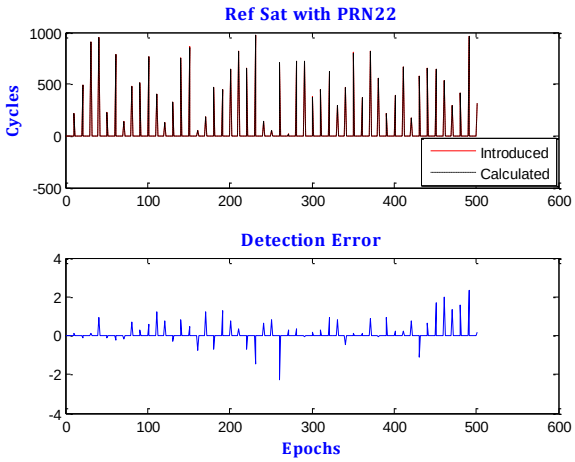


Figure 15: Moderate cycle slips Ref Sat with PRN 22

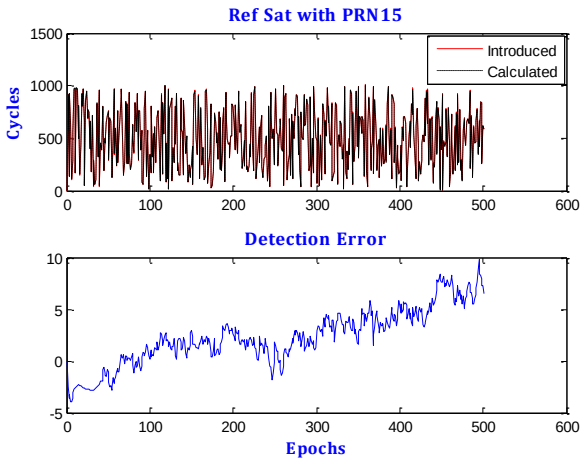


Figure 16: Intensive cycle slips Ref Sat with PRN 15

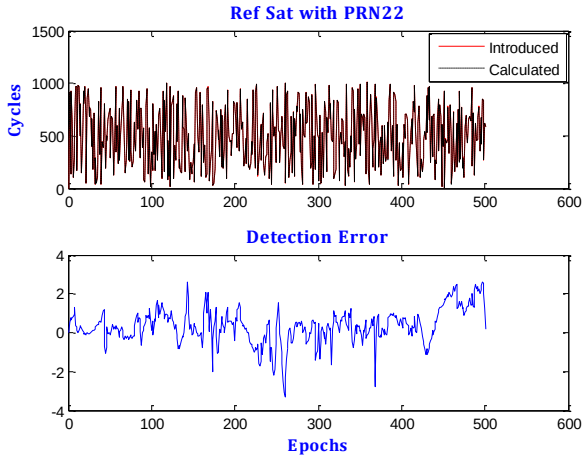


Figure 17: Intensive cycle slips Ref Sat with PRN 22

Table 3: Few slips (1 slip/100 Epochs)

| Satellite pair | Accuracy % | TD % | MD % | MSE |
|---|---|---|---|---|
| **Ref-PRN 9** | 99.72 | 100 | 93.75 | .014 |
| **Ref-PRN 14** | 99.85 | 100 | 96.03 | .008 |
| **Ref-PRN 15** | 99.14 | 100 | 98.61 | .156 |
| **Ref-PRN 22** | 99.90 | 100 | 91.07 | .002 |
| **Ref-PRN 27** | 99.40 | 100 | 98.16 | .066 |
| **Average** | 99.60 | 100 | 95.50 | .049 |

Table 4: Moderate slips (10 slip/100 Epochs)

| Satellite pair | Accuracy % | TD % | MD % | MSE |
|---|---|---|---|---|
| **Ref-PRN 9** | 99.83 | 100 | 58.33 | 0.127 |
| **Ref-PRN 14** | 99.89 | 100 | 68.55 | 0.194 |
| **Ref-PRN 15** | 99.51 | 100 | 86.59 | 1.237 |
| **Ref-PRN 22** | 99.92 | 100 | 48.45 | 0.082 |
| **Ref-PRN 27** | 99.65 | 100 | 82.87 | 0.600 |
| **Average** | 99.76 | 100 | 68.59 | 0.448 |

Table 5: Intensive slips (100 slip/100 Epochs)

| Satellite pair | Accuracy % | TD % | MD % | MSE |
|---|---|---|---|---|
| **Ref-PRN 9** | 99.84 | 100 | 0 | 1.335 |
| **Ref-PRN 14** | 99.90 | 100 | 0 | 2.122 |
| **Ref-PRN 15** | 99.52 | 100 | 0.199 | 12.816 |
| **Ref-PRN 22** | 99.93 | 100 | 0 | 0.880 |
| **Ref-PRN 27** | 99.65 | 100 | 0 | 6.242 |
| **Average** | 99.76 | 100 | 0.039 | 4.679 |

It is less likely to have very small cycle slips (e.g. 1 to 2 cycles) in the data and usually it will be hidden with the higher noise levels in kinematic navigation with low cost equipment. However, we wanted to show the accuracy of detection in this case. We chose the moderate cycle slip intensity for this test. Samples of results for introduced versus calculated cycle slips are shown in Figure 18 and Figure 19. Table 6 summarizes results for all satellites.

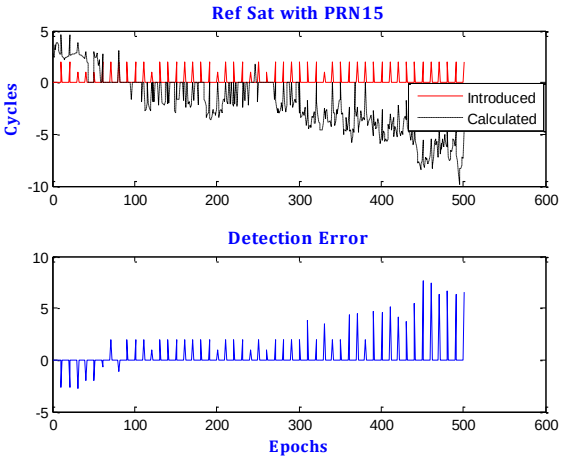


Figure 18: Small cycle slips Ref sat with PRN 15

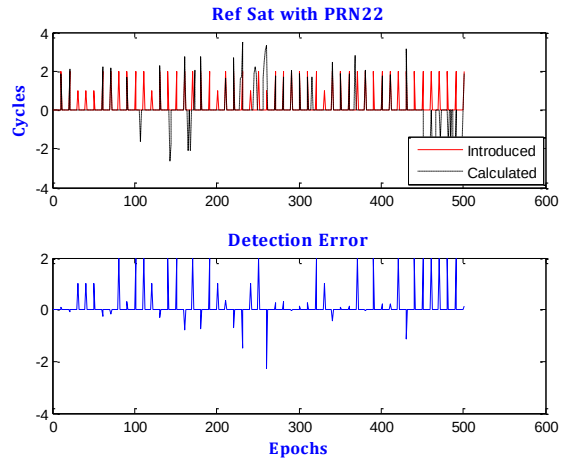


Figure 19: Small cycle slips Ref sat with PRN 22

Table 6: Small slips 1-2 cycles moderate intensity (10 slip/100 Epochs)

| Satellite pair | Accuracy % | TD % | MD % | MSE |
|---|---|---|---|---|
| Ref-PRN 9 | 26.75 | 22 | 86.41 | 0.268 |
| Ref-PRN 14 | 63.04 | 50 | 81.34 | 0.222 |
| Ref-PRN 15 | 31.46 | 48 | 90.08 | 1.202 |
| Ref-PRN 22 | 56.65 | 46 | 67.14 | 0.190 |
| Ref-PRN 27 | 6.44 | 34 | 93.43 | 0.562 |
| Average | 36.86 | 40 | 83.68 | 0.488 |

We get a moderate detection ratio and modest accuracy as the slips are of sizes close to the threshold. MSE is not far away from the case of big cycle slips but with higher misdetection ratio.

## CONCLUSIONS

The performance of the proposed algorithm was examined on several real-life land vehicle trajectories which included various driving scenarios including high and slow speeds, sudden accelerations, sharp turns and steep slopes. The road test was designed to demonstrate the effectiveness of the proposed algorithm in different scenarios such as intensive and variable-sized cycle slips.
Most of the DD phase estimations have bias and general drift trends. The bias component is mainly because of the inherited low cost inertial sensors bias. The drift is further affecting relatively lower elevation satellite-pairs. The severe ionospheric conditions involved in the trajectory and satellites geometry could contribute to this error component. Most of the sudden jumps and big concavities in error curves are coinciding with or following sharp vehicle turns and rapid tilts.
The performance of the proposed method was examined against different scenarios with different-intensity and variable-sized cycle slips. Results showed that the algorithm worked well even in the case of intensive cycle slips. In fact, the intensity of cycle slips did not affect the performance of the method. However, accuracy was slip-size dependent. We tried different slip sizes; the method showed a very high detection ratio with higher accuracy in the case of large cycle slips achieving 100% detection ration and accuracy of 99.76%. However, the accuracy was less in the case of small cycle slips with a higher mis-detection ratio. We obtained a moderate detection ratio (40%) and modest accuracy (36.86) when the slips are of sizes close to the threshold. What makes this problem less significant is that small cycle slips are less frequent than bigger ones. To sum up, results of testing the proposed method showed competitive detection rates and accuracies comparable to existent algorithms that use full MEMS IMUs. Thus with a lower cost, based on GPS/RISS integrated system, we were able to obtain a reliable phase measurement-based navigation solution. This research has a direct influence on navigation in real time applications where frequent cycle slips occur and resolving integer ambiguities is not affordable because of time and computational reasons. An additional consequence of this research is significant reduction in the cost of an integrated system due to the use of fewer MEMS sensors.

## REFERENCES


[1] B. Hofmann-Wellenhof, H. Lichtenegger and J. Collins, GPS theory and practice, New York : Springer, 1993.

[2] H. Hu and L. Fang, "GPS Cycle Slip Detection and Correction Based on High Order Difference and Lagrange Interpolation," *IEEE,* vol. 1, no. 09, pp. 384-387, 2009.

[3] A. Lipp and X. Gu, "Cycle-Slip Detection and Repair in Integrated Navigation Systems," *IEEE,* no. 2, pp. 681-688, 1994.

[4] A. El-Rabbany, Introduction to GPS -The Global Positioning System, Norwood: Artech House Inc., 2002.

[5] D. Kim and R. Langley, "Instantaneous Real-time Cycle-slip Correction of Dual-frequency GPS Data," in *International Symposium on Kinematic Systems in Geodesy, Geomatics and Navigation*, Alberta, 2002.

[6] G. Xu, GPS: Theory, Algorithms and Applications, Berlin: Springer-Verlag, 2007.

[7] T. Karamat, J. Georgy, U. Iqbal and N. Aboelmagd, "A Tightly-Coupled Reduced Multi-Sensor System for Urban Navigation," in *ION GNSS 22nd Conf*, Savannah, 2009.

[8] U. Iqbal, A. Okou and N. Aboelmagd, "An Integrated Reduced Inertial Sensor System - RISS / GPS for Land Vehicle," *IEEE,* vol. 3, no. 8, pp. 1014-1021, 2008.

[9] M. Grewal, L. Weill and A. Andrews, Global Positioning Systems, Inertial Navigation, and Integration, New Jersey: John Wiley & Sons, Inc., 2007.

[10] J. Farrell, Aided Navigation GPS with High Rate Sensors, New York: McGraw-Hill, 2008.

[11] T. Karamat, J. Georgy, U. Iqbal and N. Aboelmagd, "A Tightly-Coupled Reduced Multi-Sensor System for Urban Navigation," in *ION GNSS 22nd Conf*, Savannah, 2009.

[12] U. Iqbal, A. Okou and N. Aboelmagd, "An Integrated Reduced Inertial Sensor System - RISS / GPS for Land Vehicle," *IEEE,* vol. 3, no. 8, pp. 1014-1021, 2008.

[13] N. Aboelmagd, T. B. Karmat and J. Georgy, Fundamentals of Inertial Navigation, Satellite-based Positioning and their Integration, New York: Springer, 2012.

[14] T. Takasu and A. Yasuda, "Cycle Slip Detection and Fixing by MEMS-IMU/GPS Integration for Mobile Environment RTK-GPS," in *ION GNSS 21st Conf*, Savannah, 2008.

[15] C. Altmayer, "Cycle Slip Detection and Correction by Means of Integrated Systems," in *ION NTM Conf*, Anaheim, 2000.